



The D1-V185N mutation alters substrate water exchange by stabilizing alternative structures of the Mn₄Ca-cluster in photosystem II

Casper de Lichtenberg^{a,b}, Anton P. Avramov^c, Minquan Zhang^c, Fikret Mamedov^b, Robert L. Burnap^c, Johannes Messinger^{a,b,*}

^a Department of Chemistry, Umeå University, Linnaeus väg 6 (KBC huset), SE-901 87 Umeå, Sweden

^b Molecular Biomimetics, Department of Chemistry - Ångström, Uppsala University, POB 523, SE-75120 Uppsala, Sweden

^c Department of Microbiology and Molecular Genetics, Oklahoma State University, Stillwater, OK 74078, United States

ARTICLE INFO

Keywords:

Photosystem II
Substrate water exchange
EPR
Manganese cluster
Water oxidation
O-O bond formation

ABSTRACT

In photosynthesis, the oxygen-evolving complex (OEC) of the pigment-protein complex photosystem II (PSII) orchestrates the oxidation of water. Introduction of the V185N mutation into the D1 protein was previously reported to drastically slow O₂-release and strongly perturb the water network surrounding the Mn₄Ca cluster. Employing time-resolved membrane inlet mass spectrometry, we measured here the H₂¹⁸O/H₂¹⁶O-exchange kinetics of the fast (W_f) and slow (W_s) exchanging substrate waters bound in the S₁, S₂ and S₃ states to the Mn₄Ca cluster of PSII core complexes isolated from wild type and D1-V185N strains of *Synechocystis* sp. PCC 6803. We found that the rate of exchange for W_s was increased in the S₁ and S₂ states, while both W_f and W_s exchange rates were decreased in the S₃ state. Additionally, we used EPR spectroscopy to characterize the Mn₄Ca cluster and its interaction with the redox active D1-Tyr161 (Y_Z). In the S₂ state, we observed a greatly diminished multiline signal in the V185N-PSII that could be recovered by addition of ammonia. The split signal in the S₁ state was not affected, while the split signal in the S₃ state was absent in the D1-V185N mutant. These findings are rationalized by the proposal that the N185 residue stabilizes the binding of an additional water-derived ligand at the Mn1 site of the Mn₄Ca cluster via hydrogen bonding. Implications for the sites of substrate water binding are discussed.

1. Introduction

Photosynthesis is arguably one of the most important chemical processes on Earth. Driven by sunlight it supports aerobic life by supplying oxygen for breathing and by storing the energy of the photons in chemical bonds of, for example, lipids and carbohydrates. Mimicking and improving photosynthesis holds great promise for developing sustainable solutions for producing chemicals and fuels.

Oxygenic photosynthesis takes place in the thylakoid membranes of cyanobacteria, algae and plants. The first steps in the electron transfer reactions of photosynthesis are orchestrated by the multisubunit pigment-protein complex photosystem II (PSII). Here, in a process known as water-splitting, the energy from light is used to extract electrons and protons from water in order to reduce the plastoquinone pool and support the proton gradient across the thylakoid membrane. In this process, oxygen is released as a side product. The water-splitting chemistry occurs at a Mn₄Ca-cluster that constitutes the active site of the oxygen evolving complex (OEC), while the photochemistry and electron transfer reactions are performed by chlorophyll (Chl),

pheophytin (Pheo) and quinone cofactors as well as by a tyrosine residue [1–5].

Upon absorption of a photon in the Chl-containing antenna proteins, the excitation energy is transferred to the Chl tetramer P₆₈₀, which induces charge separation between P₆₈₀ and the nearby Pheo. The charge separation is stabilized by further electron transfer to bound plastoquinone (Q_A) and then to a terminal, exchangeable plastoquinone (Q_B). Meanwhile, the electron hole on P₆₈₀ is filled from the redox active tyrosine D1-Tyr161 (Y_Z), which in turn is reduced by an electron from the Mn₄Ca-cluster [4,6–8]. As observed first by Joliot and subsequently rationalized by Kok and Forbush, this process builds up oxidizing equivalents on a storage unit, now referred to the Mn₄Ca-cluster, in a stepwise cyclic fashion [9,10]. After every charge separation in PSII, the active site advances one step within a reaction cycle encompassing five redox states (S₀, S₁, S₂, S₃ and S₄). Dioxygen is formed and released without the need of further illumination once four oxidizing equivalents are present (S₄ state), which resets the cluster to the S₀ state. Interestingly, in the dark all states convert into the S₁ state [11–13].

* Corresponding author at: Department of Chemistry - Ångström, Uppsala University, POB 523, SE-751 20 Uppsala, Sweden.

E-mail address: johannes.messinger@kemi.uu.se (J. Messinger).

<https://doi.org/10.1016/j.bbambio.2020.148319>

Received 3 July 2020; Received in revised form 15 September 2020; Accepted 19 September 2020

Available online 23 September 2020

0005-2728/ © 2020 The Author(s). Published by Elsevier B.V. This is an open access article under the CC BY license (<http://creativecommons.org/licenses/by/4.0/>).

During the S-state cycle, two substrate water molecules bind to the Mn_4Ca cluster as H_2O or OH^- , and are further deprotonated to then be oxidized during the formation of the $\text{O}=\text{O}$ double bond during the $\text{S}_4\text{-S}_0$ transition. While there are a number of techniques to detect bound water molecules at the Mn_4Ca cluster [14–18], the only approach that can identify them as substrate is rapid $\text{H}_2^{18}\text{O}/\text{H}_2^{16}\text{O}$ isotope exchange in conjunction with light-induced O_2 formation and detection via time-resolved membrane-inlet mass spectrometry (TR-MIMS) [19–22]. From the isotopic composition of the oxygen produced after a variety of incubation times with H_2^{18}O two distinct kinetic incorporation rates of ^{18}O can be derived that typically differ by more than an order of magnitude (reviewed in [16,23–25]). These rates have been assigned to the exchange of the two substrate waters, which are referred to as fast (W_f) and slow (W_s) exchanging substrates. Both substrate waters have been shown to bind to the Mn_4Ca cluster in the S_2 and S_3 states, while only the slower exchanging substrate water has been kinetically resolved to bind in the S_0 and S_1 states. We note that there are no good reasons to assume that W_f is not bound in the S_0 and S_1 states, as the structure of the Mn_4Ca cluster remains similar and no water binding events are suggested to occur between the S_0 and S_2 states [16,18,26–29]. High-resolution crystallographic data have identified that there are four terminal water ligands bound to the active site, in addition to the five oxo-bridges (Fig. 1) [30]. Additionally, a water insertion has been observed to occur during the S_2 to S_3 state transition, adding an additional water moiety to the mix of possible substrates

[16,18,27,29,31]. Previous TR-MIMS experiments and DFT calculations have identified the central O5 bridge as the most likely candidate for W_s [24,32]. More recent H_2^{17}O labelling experiments coupled with EDNMR detection demonstrate that O5 exchanges with bulk water at a rate compatible with the rates measured for W_s by TR-MIMS [15,33,34]. The exchange of this central bridge is proposed to require the equilibrium between several conformations of the Mn_4Ca -cluster in each S state [35–37].

A common approach to further understand and characterize the water splitting mechanism in PSII has been to study the effects of selected mutations in the vicinity of the Mn_4Ca -cluster. Typically, these mutants are screened for alterations in the kinetics of water oxidation and for changes in the spectroscopic fingerprints of PSII. This usually includes measurements of proton and oxygen release kinetics, S_i state transitions by Joliot type measurements, substrate exchange kinetics, changes in FTIR and of course changes in the EPR spectra (for review see [16,38,39]).

The D1-V185 residue has been the focus of several recent experimental and theoretical studies [40–45]. The V185 residue is located adjacent to the cluster near three potential substrate candidates (W_2 , W_3 and W_4). It may also block or regulate the access to the open coordination site at Mn1 (Fig. 1). In PSII from *Synechocystis* sp. PCC 6803, mutation of the D1-V185 to the polar residue asparagine (N) slows down the release of O_2 from 1.2 ms to about 27 ms half-time (27 °C). On the other hand, mutation of V185 to threonine resulted in only a modest

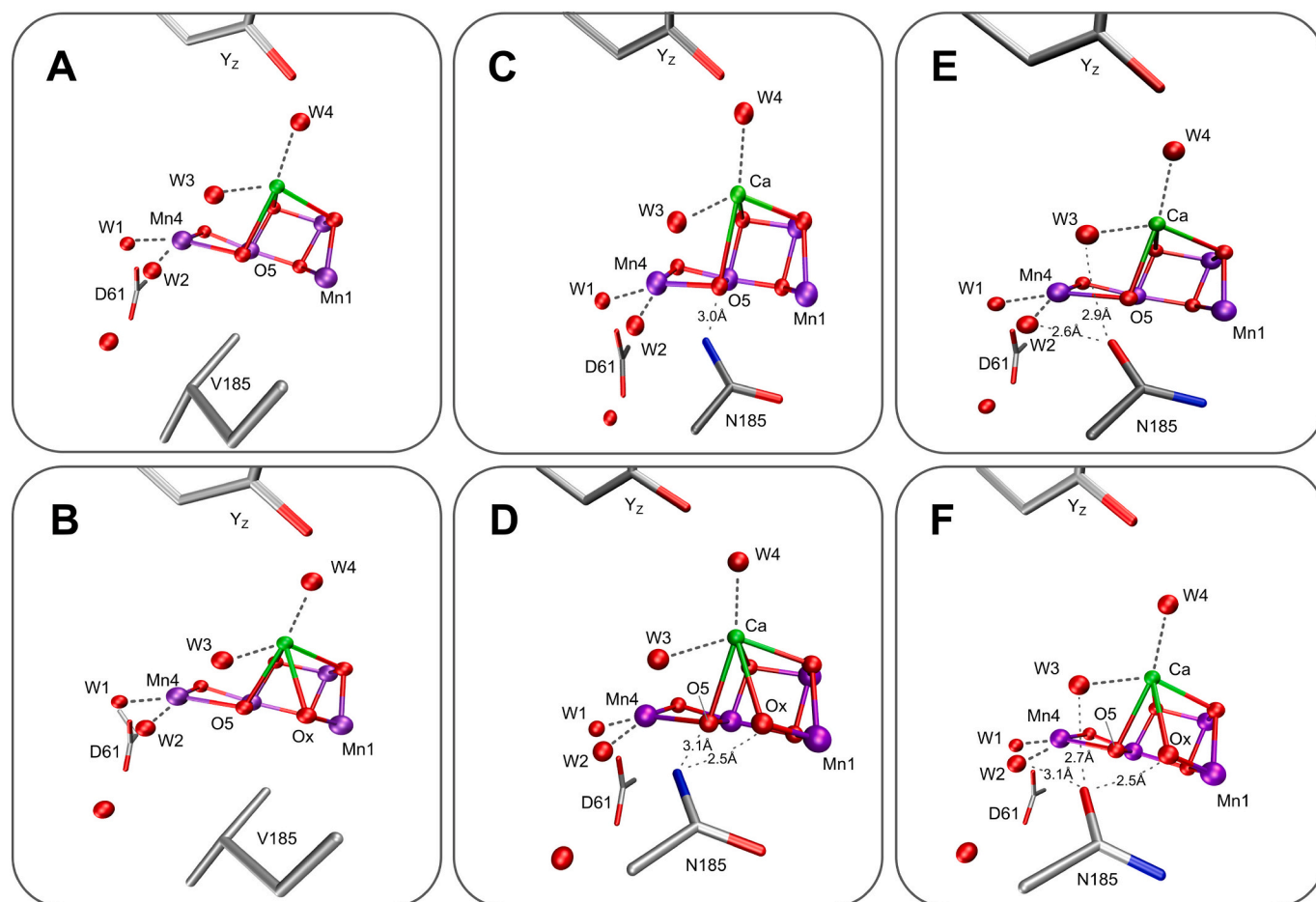


Fig. 1. Molecular representation of the D1-V185 residue in the vicinity of the Mn_4Ca -cluster. A & B: native structures of V185 and the Mn_4Ca cluster in the S_1 state displaying the S_2^A conformation (PDB: 6DHE) and the S_3 state displaying the S_3^{AW} conformation (PDB: 6DHO), respectively, along with the Y_z and D1-D61 residues. C, D, E & F: Models of the mutated N185 residue in the vicinity of the Mn_4Ca cluster, with either the amide nitrogen or the carboxo pointing towards the Mn_4Ca -cluster. Indicated distances, between the nitrogen or oxygen atom on the N185 residue and the oxygen atom of potential substrate waters were estimated with WinCoot.

effect on the oxygen release (from 1.2 ms to 1.5 ms) [40]. In a follow up study, the pH dependence of this final step was investigated in the V185N mutant and compared to the D1-D61N and D1-D61A mutants that exhibit similar delays in the O_2 release, but are known to impair proton extraction [41]. It was shown that the pH dependence of the O_2 release kinetics was different between the D61 and V185 mutants. D61N and D61A show significant changes in the O_2 release kinetics when the pH is altered from 5.5 to 7.5, while the kinetics in the V185N mutant were only slightly affected. This indicates that in case of V185 it is not directly the proton extraction that slows O_2 release, but possibly it is the reorganization of the water and/or protons that has to occur during the $S_3 \rightarrow S_4 \rightarrow S_0$ transition that is affected by the V185N mutation [41]. FTIR measurements showed that mutating valine 185 to asparagine leads to extensive changes in the hydrogen bonding network in the area between Y_Z and D61, yet without affecting the direct hydrogen bonding partners of D61. Importantly, the authors identified perturbations of Ca-bound W3, while they found that the hydrogen bonding network of W2 was only slightly affected [42].

Electron paramagnetic resonance (EPR) spectroscopy is a sensitive method to study the OEC of PSII. This method can be employed to probe the electronic spin states of the Mn_4Ca -cluster during its turnover and the coupling to the tyrosine radical in its vicinity (Y_Z). EPR signals can be induced and studied in every S state of the Kok cycle [46–48], and are sensitive to the conformation of the Mn_4Ca cluster. Two of the most prominent signals in PSII are the S_2 state low spin (LS) multiline (ML) signal around $g \sim 2$ and its high spin (HS) counterpart in the $g \sim 4$ region [49–52]. The S_2^{LS} signal arises from the open cube structure containing a five-coordinate $Mn1(III)$ ion which we will refer to as S_2^A (Fig. 2), while the conformation of the S_2^{HS} state is controversial. It has been suggested to be either (i) a closed cubane where the bond between $Mn4$ and $O5$ is moved to be between $Mn1$ and $O5$ along with a valence swap between $Mn1$ and $Mn4$ (S_2^B) [36,53–56], (ii) to have a similar structure to S_3 with a hydroxo bound to $Mn1$ (S_2^{AW}) [37,43,45,57], or to (iii) have a protonated $O4$ bridge (S_2^{PI}) [58].

Recent studies based on extended X-ray absorption fine spectroscopy (EXAFS) suggest that the $Mn-Mn$ and $Mn-O$ distances obtained for the S_2^{HS} state do not agree with the closed cubane model, but it remains to be shown if they agree better with models (ii) or (iii) [57,60,61].

The V185T mutant in *Thermosynechococcus elongatus* was found to have a significant fraction of its Mn_4Ca -clusters in the S_2^{HS} state [44]. Furthermore, the authors describe that the proton release appears to behave differently from wild type (WT), so that protons are released in a 1:1:1:1 fashion during the S state cycle rather than in the canonical 1:0:1:2 fashion (starting the count from $S_0 \rightarrow S_1$).

One theoretical study found that by rotating the V185 residue away from the position determined by crystallography the insertion of water from calcium onto $Mn1$ becomes easier and occurs in the sub-microsecond time-scale rather than the millisecond timescale [43]. Therefore, V185 potentially has a rather large effect on water insertion in the S_2 to S_3 transition, and possibly also for substrate water exchange in the S_3 state. As a consequence, mutations of this residue may be expected to lead to rather extensive effects on the substrate exchange process.

We have investigated here how the D1-V185N mutation in *Synechocystis* sp. PCC 6803 affects the exchange kinetics of substrate water with ^{18}O -labelled bulk water in the S_1 , S_2 and the S_3 states using TR-MIMS. Additionally, we studied the effects of this mutation on the EPR properties of the Mn_4Ca -cluster and its interaction with Y_Z in the S_1 , S_2 and S_3 states by EPR spectroscopy.

2. Methods

2.1. Isolation of thylakoid membranes

Synechocystis sp. PCC 6803 thylakoid membranes were isolated at 4 °C under dim green light [62]. Cells were harvested at $10,000 \times g$ and

washed in 50 mM 4-(2-hydroxyethyl)-1-piperazineethanesulfonic acid (HEPES)-NaOH (pH 7.3), 30 mM NaCl. Then cells were pelleted at $12,000 \times g$ and resuspended in a ~ 120 mL of 1.2 M betaine, 50 mM 2-(N-morpholino)ethanesulfonic acid (MES)-NaOH (pH 6.0), 10% (v/v) glycerol, 5 mM $CaCl_2$ and 5 mM $MgCl_2$ and kept at 4 °C in the dark for 1 h. Shortly before breaking the cells, the following additions were made to the cell suspension: 1 mM benzamidine, 1 mM ϵ -amino-n-caproic acid, 1 mM phenylmethylsulfonyl fluoride, and 0.05 mg/mL DNase I. The cells were broken by 9 cycles of 15 s ON and 5 min OFF in a glass bead homogenizer (Bead-Beater, BioSpec Products, Bartlesville, OK) with 0.1 mm glass beads. After breakage, the sample was centrifuged at $5000 \times g$ to separate unbroken cells, cell debris and residual glass beads. The supernatant containing a mix of thylakoid membranes and soluble proteins was concentrated by ultracentrifugation (35 min at $125,000 \times g$) and suspended in 1.2 M betaine, 50 mM MES-NaOH (pH 6.0), 10% (v/v) glycerol, 20 mM $CaCl_2$ and 5 mM $MgCl_2$ to a concentration of 1.0–2.0 mg of Chl/mL. Chl a concentration was determined in triplicates by extraction in methanol using the extinction coefficients as described in [63]. Concentrated thylakoid membranes from wild-type cells were flash frozen as 5–7 mL aliquots in liquid nitrogen and stored at -80 °C for further use. D1-V185N thylakoid membranes were immediately used for preparation of PSII core complexes without freezing.

2.2. Purification of PSII core complexes

PSII core complexes were purified from thylakoid membrane isolates at 4 °C under dim green light [62]. The detergent n-dodecyl- β -D-maltoside (Anatrace Inc., Maumee, OH) was added dropwise from a 10% (w/v) stock to the suspension of thylakoid membranes (50–60 mg of Chl) to a final concentration of 1% (w/v) of detergent and ~ 1 mg/mL of Chl [64]. The solubilization of the thylakoid membranes was performed by gently stirring the suspension in the dark for 10 min. The suspension was centrifuged at $40,000 \times g$ for 20 min at 4 °C to separate unsolubilized material. The supernatant was loaded at the flowrate ~ 3 mL/min to a 40 mL Ni-NTA Superflow affinity resin (Qiagen, Inc.) that had been packed in a 5 cm diameter chromatography column and equilibrated with B_0 buffer [1.2 M betaine, 50 mM MES-NaOH (pH 6.0), 10% (v/v) glycerol, 20 mM $CaCl_2$ and 5 mM $MgCl_2$, 0.03% n-dodecyl- β -D-maltoside]. The column was washed with 4 column volumes B_0 buffer at a flow rate of 5 mL/min or until the $A_{420} \leq 0.35$ and then eluted with four column volumes of B_0 buffer containing 50 mM histidine. EDTA was added to the eluent to a final concentration of 1 mM. The eluent was concentrated by ultrafiltration in a stirred ultrafiltration cell with a 100 kDa cutoff membrane (Ultracel disk, NMWL 100 kDa, Millipore Sigma, Germany) under 60 psi N_2 at 4 °C followed by Amicon Ultra-15,100 K centrifugal filter column (Millipore Sigma, Germany) to approximately 1 mg of Chl/mL. The concentrated PSII complexes were flash-frozen in liquid N_2 as 100 μ L aliquots and stored at -80 °C until used.

2.3. Substrate-water exchange measurements with time resolved membrane inlet mass spectrometry

The substrate-water exchange rates of PSII core complexes were measured using an isotope ratio mass spectrometer (Finnigan Delta Plus XP). A 165 μ L rapid mixing reaction cell was connected to the spectrometer with a stainless steel pipe, passing through a Dewar filled with liquid N_2 [19,21,22,65,66]. An aliquot of 100 μ L PSII (~ 1 mg/mL Chl) was thawed on ice on the day of the measurement. The aliquot was washed in 50 mM MES-NaOH pH 6.5, 1 M betaine, 15 mM $CaCl_2$, 15 mM $MgCl_2$ using an Amicon Ultra-0.5 centrifugal filter unit (100 kDa cutoff) for $125 \times$ dilution of the original buffer. Finally, the sample was diluted to a concentration of app. 0.2 mg/mL Chl and split in two 1.5 mL glass vials and each vial was administered a single saturating flash through the bottom with a xenon flash lamp (5 μ s FWHM). The

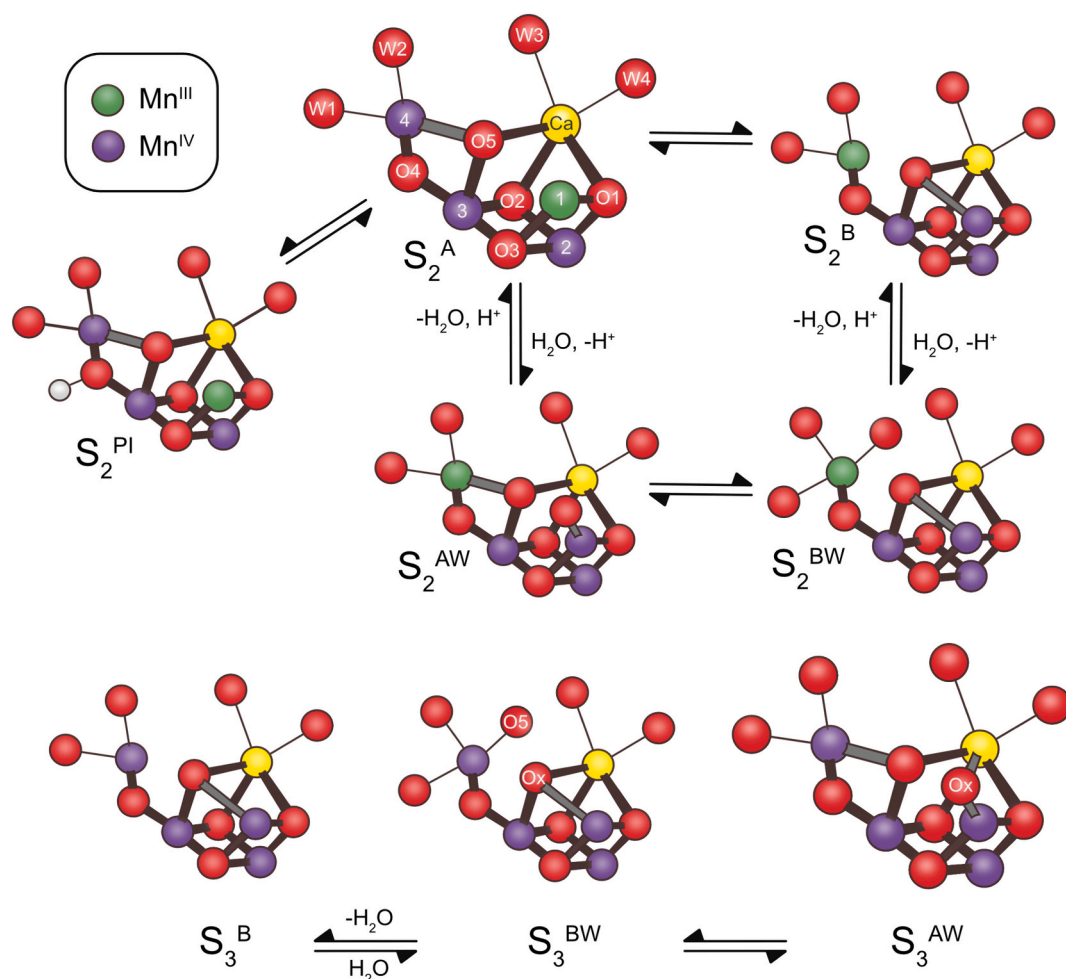


Fig. 2. The Mn_4Ca -cluster in the conformations known from crystallography along with alternative conformers that have been suggested based on spectroscopy and DFT calculations. Open cube structures are designated A, while closed cube structures are designated B. W indicates an additional water or hydroxide bound to the cluster. PI indicates a proton isomer. Mn^{III} ions are displayed in green, Mn^{IV} are shown in purple, oxygens are colored red and calcium is displayed in yellow. The structures of S_2^{A} and S_3^{AW} were observed by crystallography [18,29]. While the S_2^{A} structure has been attributed to the LS multiline signal, there are different proposals for the conformation relating to the S_2^{HS} signal. The S_2^{B} conformation [51], the water bound S_2^{AW} [41,55,71] and the proton isomer S_2^{PI} [56]. The S_2^{BW} conformation was suggested as an intermediate conformation in the transition from S_2 to S_3 [57,90]. The S_3^{B} and S_3^{BW} conformations were suggested based on EDNMR experiments [90].

samples were stored on ice in the dark until approximately 1 h before measurement when a sample was moved to room temperature for dark-adaptation. 20 min before the measurement, 2,6-dichloro-1,4-benzoquinone was added to the sample from a 200 mM stock in dimethylsulfoxide (DMSO) to a final concentration of 0.25 mM. For the S_1 state measurements, 2 mM $\text{K}_3[\text{Fe}(\text{CN})_6]$ was added to facilitate the fast transition from S_1 through the cycle to S_0 by oxidizing the non-heme iron to Fe^{3+} . The sample was loaded into the reaction cell under dim green light and was degassed for 20 min in the dark at 15 °C. 5 min prior to the measurement, a modified gas-tight syringe (Hamilton CR-700-50), previously loaded under N_2 atmosphere with 22 μL 97% H_2^{18}O , was quickly inserted into the reaction cell to avoid gas exchange with air. To minimize the O_2 content in the H_2^{18}O water, it was bubbled with N_2 for 15 min through a septum prior to being transferred into a N_2 -glovebox for storage. Residual O_2 was measured by repeated injections into the reaction cell, yielding a calibration curve (Supplemental Fig. 1) used for correction of the injection artifact (supplemental methods). The syringe was connected to a nitrogen line (7 bar) via a fast switching solenoid valve to allow rapid injection and mixing of the labelled water (mixing was complete after ~ 6 ms, based on fluorescence measurements with injections of fluorescein, performed as described in [19,67,68]). The measurement sequence for each S state is shown in

Supplemental Fig. 2, which was adapted from [69]. The final H_2^{18}O concentration was estimated from the m/z 34: m/z 36 ratio of the O_2 produced by the final (normalizing) flash group and found to be 13.3%.

The substrate exchange rates (k_f and k_s) for the fast and slow substrate waters were determined by a simultaneous fit of the m/z 34 and the m/z 36 data to Eqs. (1) and (2), as described in [19,65]. In our recent publication we described an exchange phase belonging to W_s of intermediate speed. We found no need to include this phase here. The parameter a is the ratio of the amplitudes of the fast and slow phases of substrate water exchange in the $^{34}\text{O}_2$ data. The parameter a was determined from the initial enrichment (α_{in}) and the final enrichment (α_{f}) as shown in Eq. (3). The initial enrichment was found to be 0.7%, i.e. slightly elevated over natural abundance as a result of leakage from the syringe tip.

$$m/z\ 34 = a \cdot (1 - e^{-k_f t}) + (1 - a) \cdot (1 - e^{-k_s t}) \quad (1)$$

$$m/z\ 36 = 1 - e^{-k_s t} \quad (2)$$

$$a = \frac{\alpha_f \cdot (1 - \alpha_{\text{in}}) + (1 - \alpha_f) \cdot \alpha_{\text{in}}}{(1 - \alpha_f) \cdot \alpha_f \cdot 2} \quad (3)$$

Corrections for sample dilution and isotopic enrichment were not required ([19]), since all measurements were taken after full mixing

was achieved (> 6 ms). The delay of 4 ms between the trigger pulse and the start of injection was accounted for.

2.4. EPR spectroscopy

EPR samples were prepared by washing of the PSII core complexes in 50 mM MES-NaOH pH 6.5, 1 M betaine, 15 mM CaCl_2 , 15 mM MgCl_2 using an Amicon Ultra-0.5 with a cutoff of 100 kDa. The samples for ammonia binding in the S_2 state were washed with 50 mM HEPES-NaOH pH 7.6, 1 M betaine, 15 mM CaCl_2 , 15 mM MgCl_2 . All samples were supplemented with 1 mM ethylenediaminetetraacetic acid (EDTA) and 1 mM phenyl-1,4-benzoquinone (PPBQ; in DMSO). When indicated, ammonium chloride was added from a 2 M stock solution in the experimental buffer to a final concentration of 100 mM. The final Chl concentration of EPR samples was 2.3–2.7 mM.

EPR samples in 4 mm quartz EPR tubes were pre-illuminated for one minute under continuous room light while shaking, followed by 60 minute dark adaptation at room temperature. The S_1 state samples were flash frozen immediately after dark-adaptation. To achieve predominantly the S_2 and S_3 states, samples were administered one or two saturating laser flashes (at 525 nm, 7 nsec, 800 mJ and 2 Hz) from a Nd-YAG laser (Spectra Physics, USA) and then immediately flash frozen in a dry ice/ethanol bath and transferred to liquid N_2 for storage before the measurements.

Low temperature continuous wave EPR measurements were performed with an X-band EMX Micro spectrometer equipped with a EMX Premium bridge and ER4119HS resonator (Bruker BioSpin, Germany). The system was fitted with an Oxford 900 cryostat and an ITC-503 temperature controller from Oxford instruments Ltd., UK. The split S_1 EPR signal was induced by continuous illumination at 5 K directly into the EPR resonator via a light guide coupled to the output of a 800 W projector lamp that was filtered through 5 cm CuSO_4 (aq). The split S_3 EPR signal was induced either the same way as the split S_1 signal or by illumination at 5 K by 830 nm NIR light from a LQC830-135E continuous laser diode (Newport, USA) for 40 min. When indicated, the S_2 state ML signal was induced by illumination at 200 K for 6 min. Processing and analysis of EPR spectra was performed in Bruker Xepir 2.1 software.

3. Results

3.1. H_2^{18}O substrate exchange with TR-MIMS

We investigated the exchange rates of substrate waters bound at the Mn_4Ca -cluster with bulk water in PSII core complexes isolated from *Synechocystis* sp. PCC. 6803 WT-cells and from the D1-V185N mutant by TR-MIMS.

The experimental data obtained at mass-to-charge ratios 34 and 36 in the S_1 , S_2 and S_3 states of the Kok-cycle at pH 6.5 and 15 °C are shown in Fig. 3. For clarity, data normalized to the O_2 levels reached after full exchange are displayed. The isotopic enrichment calculated from these final levels using the $^{34}\text{O}_2/^{36}\text{O}_2$ ratio corresponded closely to that determined from the four normalizing flashes (for details see SI). This indicates that all centers participate in substrate water exchange. Each data point in Fig. 3 represents the exchange of one (Fig. 3A, C, E; $^{16,18}\text{O}_2$) or two substrate waters (Fig. 3B, D, F; $^{18,18}\text{O}_2$) after a given incubation time with H_2^{18}O enriched water.

For both WT- and V185N-PSII, the typical biphasic rise in the $^{16,18}\text{O}_2$ signal measured at m/z 34 is observed in the S_1 , S_2 and S_3 states. These two phases are interpreted, as previously [19,65], to arise from two distinct substrate water molecules, the fast exchanging W_f and the slow exchanging W_s . The corresponding rates of isotope exchange with the bulk water are referred to as k_f and k_s and are shown in Table 1. The $^{18,18}\text{O}_2$ signal, measured at a mass to charge ratio of m/z 36, displayed a monophasic rise with a first order rate constant that corresponded to the slower of the two phases in the $^{16,18}\text{O}_2$ signal. The $^{16,18}\text{O}_2$ and

$^{18,18}\text{O}_2$ traces were fitted simultaneously using Eqs. (1) and (2), see lines in Fig. 3. The WT-PSII exchange rates are in good agreement with those previously reported, taking into account that there are differences in temperature and buffer conditions [70,71].

The rate constants for fast and slow substrate water exchange collected in Table 1 show that the V185N and WT-PSII had a similar overall S state dependence: the exchange of W_s is faster in the S_2 state than in the S_1 and S_3 states. Interestingly, the W_s exchange was found slowest in the S_1 state for the WT, while it was slowest in the S_3 state for the V185N mutant, as the exchange was retarded by a factor of ~ 9 as compared to the S_2 state for V185N, but only by a factor of ~ 2 for the WT. In agreement with earlier data, the exchange of W_f is too fast to be detected in the S_1 state for both WT and V185N, but can be resolved in the S_2 state. Similar to the exchange of W_s , the S_3 formation led to a slowing of the W_f exchange by a factor of ~ 6 in V185N and ~ 3 in the WT as compared to S_2 .

Despite this overall similar trend in the S state dependence of the substrate exchange in WT and V185N, highly interesting differences between the two sample types are revealed by a closer inspection of the data in Fig. 3 and Table 1. In the S_1 and S_2 states, the V185N mutant displayed a 2–4-fold faster W_s exchange than the WT sample, while this order was reverse in the S_3 state, where the W_s exchanged two times faster in WT- than in V185N-PSII.

Remarkably, exactly the same ratio between fast water exchange in the V185N mutant and WT was obtained in the S_3 state, while the V185N/WT substrate exchange rate ratios in the S_2 state differed for W_f and W_s (Fig. 3, Table 1).

3.2. EPR spectroscopy

Since we showed recently that the substrate exchange rates depend on the configuration of the Mn_4Ca cluster [37], we recorded EPR spectra of the S_2 states in WT-PSII and V185N-PSII core preparations to gain insight into their dominant configuration. Similarly, it was suggested that Y_Z plays a key role in the S_3 state substrate exchange mechanism by transiently donating an electron to the Mn_4Ca -cluster to generate an S_2Y_Z state [35]. To probe if the coupling of Y_Z to the Mn_4Ca -cluster is perturbed by the V185N mutation, split EPR signals were measured in the S_1 and S_3 states. These signals arise from the magnetic coupling of Y_Z , which was induced by ~ 5 K illumination with visible or IR light, with the Mn_4Ca -cluster [72].

Fig. 4 shows the split S_1 EPR spectrum from the WT-PSII and V185N-PSII core preparations. Very similar EPR signal shapes and intensities were observed in both samples around 3280 G ($g = 2.043$). This indicates that Y_Z is magnetically coupled to the Mn_4Ca -cluster in a similar way in both WT- and V185N-PSII, and that the S_1 state is in the same spin state.

In the WT PSII cores, a laser flash given at room temperature induced the typical S_2 EPR multiline signal that is centered at $g \sim 2.0$ and has a hyperfine splitting of ~ 88 gauss (black spectrum in Fig. 5A). By contrast, the intensity of the multiline signal is ~ 10 times weaker in the V185N mutant, and the hyperfine splitting appeared to be more compressed than in the WT with a peak-to-peak distance of ~ 70 gauss. No obvious $g \sim 4.1$ or other high spin species were detected under our conditions that can be attributed to the Mn_4Ca -cluster in either WT- or V185N-PSII, even if illumination with unfiltered white light (combination of 200 K and IR) was employed (see Supplemental Fig. 3). We note that the generation of the $g = 4.1$ signal in *Synechocystis* was rarely possible, as summarized in [73], and only reported once for WT-PSII [74]. The only experimental difference between the conditions in Ref 74 and ours is the use of betaine instead of glycerol, so either the presence or absence of one of these cryoprotectants, or a difference in sample preparation might be responsible for the different observations.

This indicates that in the V185N-PSII either very little of a slightly modified S_2 state was formed in the mutant and the rest of the sample remained in the S_1 state, or that most of the S_2 formed is in an EPR

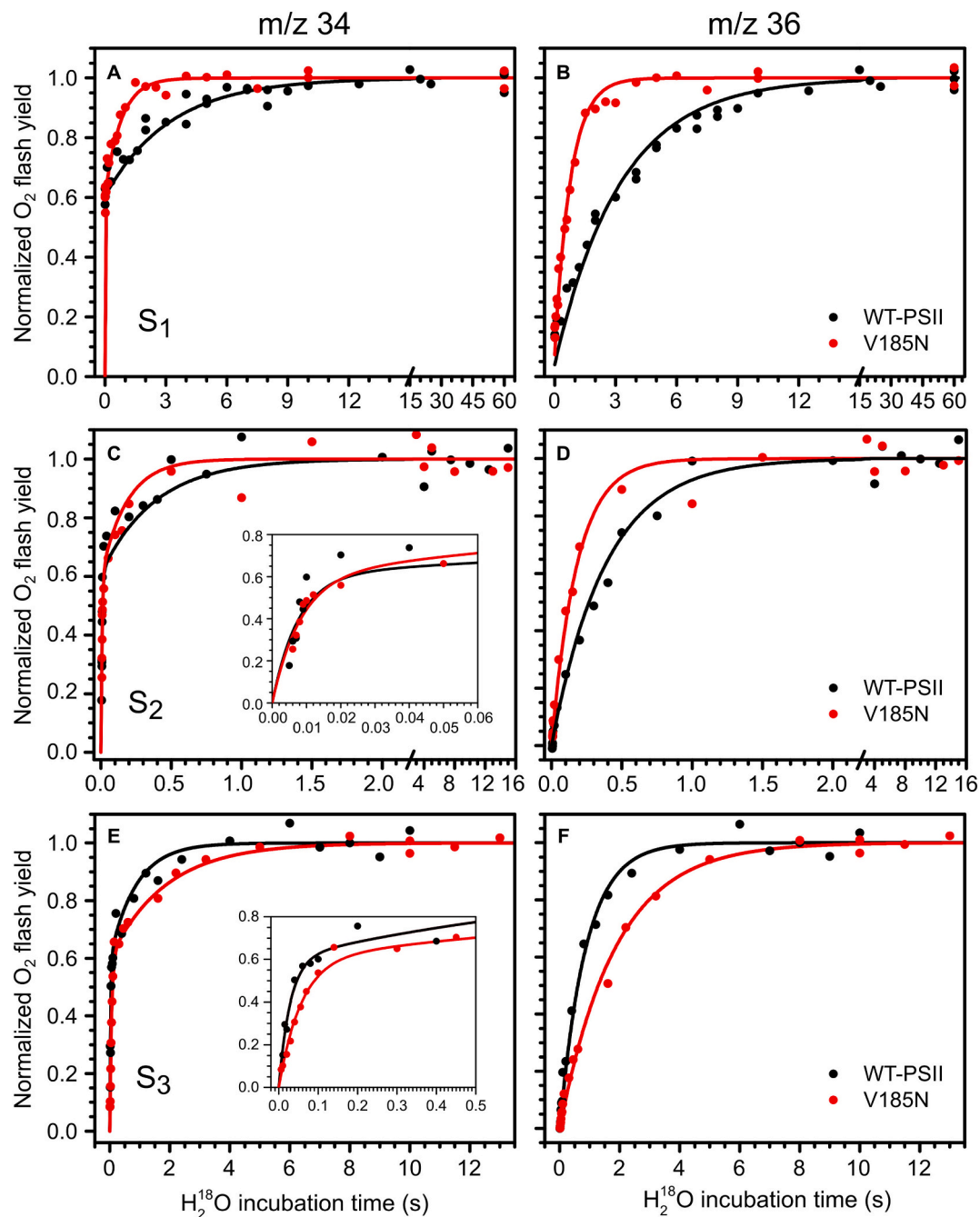


Fig. 3. $\text{H}_2^{18}\text{O}/\text{H}_2^{16}\text{O}$ substrate water exchange in the S_1 , S_2 and S_3 states of WT-PSII (black traces) and V185N-PSII (red traces) at pH 6.5 and 15 °C. A, C and E display single-labelled O_2 (m/z 34) yields obtained after discrete incubation times with H_2^{18}O . Panels B, D and F display the simultaneously recorded double-labelled O_2 (m/z 36) signals. Dots represents measurements, while solid lines represent kinetic fits of the exchange rates (Table 1). For clarity of presentation, different time axes were selected for displaying the data obtained in the three S states. Inserts show an enlarged view of the fast phase of water exchange in the m/z 34 data.

Table 1

Rate constants and their errors obtained from global fits of the $^{16,18}\text{O}_2$ and $^{18,18}\text{O}_2$ data obtained in substrate water exchange experiments (Fig. 2) of WT-PSII core complexes from *Synechocystis* sp. 6803 and of the corresponding V185N-PSII mutant at 15 °C and pH 6.5.

S state	WT-PSII		V185N-PSII		V185N/WT	
	k_f	k_s	k_f	k_s	k_f	k_s
S_1	-	$0.33 \pm 0.01 \text{ s}^{-1}$	-	$1.45 \pm 0.09 \text{ s}^{-1}$	-	4.4 ± 0.3
S_2	$132 \pm 14 \text{ s}^{-1}$	$2.6 \pm 0.2 \text{ s}^{-1}$	$121 \pm 12 \text{ s}^{-1}$	$5.5 \pm 0.4 \text{ s}^{-1}$	0.9 ± 0.1	2.1 ± 0.2
S_3	$35 \pm 3 \text{ s}^{-1}$	$1.15 \pm 0.06 \text{ s}^{-1}$	$17.7 \pm 0.9 \text{ s}^{-1}$	$0.59 \pm 0.05 \text{ s}^{-1}$	0.51 ± 0.05	0.51 ± 0.05
S_1/S_2	-	0.12 ± 0.01	-	0.25 ± 0.02	-	-
S_2/S_3	3.1 ± 0.4	2.3 ± 0.2	5.9 ± 0.7	9 ± 1	-	-

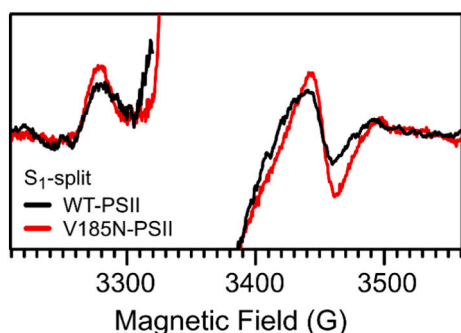


Fig. 4. Light-dark EPR spectra, displaying the split- S_1 signals of WT-PSII (black) and V185N-PSII (red) induced by visible illumination. The overmodulated Y_D radical signal in the center of the spectrum was removed for clarity.

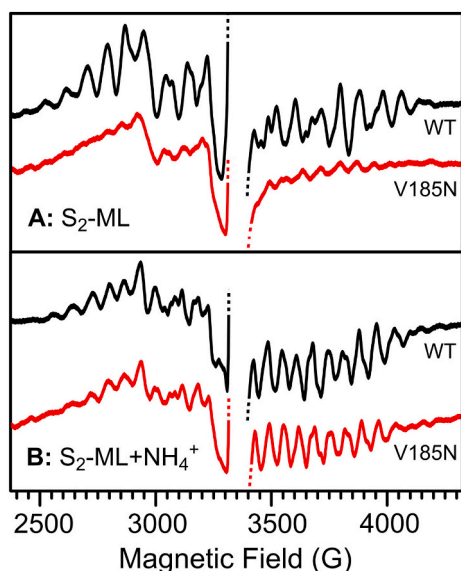


Fig. 5. S_2 state ML EPR signals recorded of WT-PSII (black) and V185N-PSII (red) after one laser flash. Microwave frequency: 9.38 GHz, microwave power 20 mW, modulation amplitude 20 G, temperature 7 K. A: Samples measured at pH 6.5. B: Samples measured in the presence of 100 mM of NH_4Cl at pH 7.6. The over modulated Y_D radical signal in the middle of all spectra was cut out for clarity. All spectra were normalized to their Chl concentrations.

invisible state. Both interpretations imply a changed conformation of the Mn_4Ca cluster in at least the S_2 state. Assuming that at 200 K no structural changes can take place, the S_1 state in the V185N mutant also has a different conformation than that of the WT. This may be reconciled with the S_1 split signal data if one assumes that this different conformation has the same total spin as the WT S_1 state conformation.

Recently, it was shown that the presence of ammonia stabilizes the Mn_4Ca -cluster in the conformation that gives rise to the S_2^{1S} ML signal [75]. Thus, we measured the S_2 state ML signal in WT- and V185N-PSII in presence of 100 mM ammonia at pH 7.6. This pH was chosen to have an effective ammonia concentration of approximately 1 mM available for binding to the Mn_4Ca cluster. Fig. 5B shows that under these conditions EPR multiline signals of nearly identical amplitude were found for WT- and V185N-PSII that show the typical appearance of the ammonia modified S_2 ML signal. The ammonia data suggest that also in absence of ammonia the S_2 state was formed in both samples to about the same extent by the laser flash, but that the Mn_4Ca -cluster is in an EPR 'invisible' conformation in the V185N mutant, likely some HS form.

The WT-PSII core preparations show the typical S_3 EPR split signal [76] signified by a main radical peak at $g \sim 2$ having a width of 19.4 G

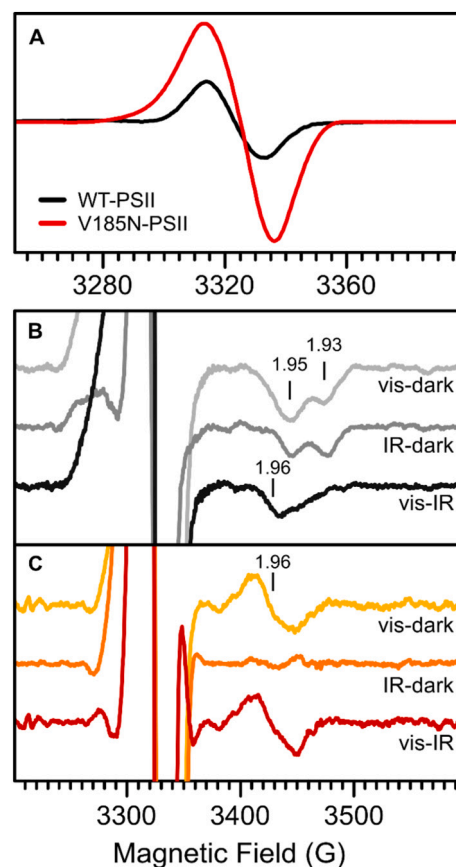


Fig. 6. Analysis of the S_3 -split EPR signals in WT- and V185N-PSII. A, induction of the Y_2 radical by NIR-illumination in WT-PSII (black) and V185N (red). B, split signal induction in the S_3 state of WT-PSII with visible light (light grey), NIR (grey) and the visible-NIR difference (black). C, split signal induction in the S_3 state of V185N-PSII with visible light (yellow), NIR (orange) and the visible-NIR difference (red). Selected g -values for the split signal (1.93 and 1.95) and the $Q_A^-Fe^{2+}$ signal (1.96) are indicated with vertical bars.

(IR-illuminated) and two troughs at $g = 1.93$ and $g = 1.95$ (Fig. 6B). Subtraction of the IR induced split signal from the visible light induced split EPR spectrum reveals the $Q_A^-Fe^{2+}$ signal at $g = 1.96$, evidencing the successful charge separation at 5 K under visible illumination. In V185N-PSII the central radical signal induced by IR-illumination was more than 2 times as intense as that observed for the WT (Fig. 6A). In addition, the signal was broadened by approximately 3 G and shifted by roughly 2 G as compared to the WT spectrum. In D1-V185N samples, the typical troughs at $g = 1.93$ and $g = 1.95$ were neither observed with IR nor visible illumination, although the $Q_A^-Fe^{2+}$ signal at $g = 1.96$ confirmed charge separation with visible light (Fig. 6C). These data indicate that the D1-V185N mutation infers significant changes in either the coupling of Y_2 with the Mn_4Ca cluster or to the spin state and thus conformation of the Mn_4Ca cluster in the S_3 state. These options will be discussed below in conjunction with the TR-MIMS data.

4. Discussion

In this study, we investigated the substrate exchange rates of PSII core complexes, with the D1-V185N mutation, in the S_1 , S_2 and S_3 states of the Kok cycle and compared them to the exchange rates determined for the WT-PSII. In addition, we examined how the V185N mutation affected the EPR properties of the Mn_4Ca -cluster in the S_2 state, and magnetic coupling of the Mn_4Ca cluster with the redox-active amino acid residue Y_2 in both the S_1 and S_3 states.

We found the largest relative change for the W_s exchange rate in the

S_1 state, where W_s exchanged four times faster in the mutant than in the WT. A similar trend was observed for the mutant in the S_2 state, albeit W_s exchange was accelerated only by a factor of two. Interestingly, we did not observe any significant effects of the mutation on the W_f exchange rate in the S_2 state. Importantly, the results were completely different for the S_3 state: here, the exchange rates of both W_s and W_f were slower by the factor of two in V185N-PSII as compared to WT-PSII.

The EPR measurements revealed that the V185N mutant has a modified S_2 state structure, and by inference from the substrate exchange and 200 K illumination data, the same may be true for the S_1 state. In the S_3 state, either the coupling between Y_Z and the Mn_4Ca cluster is perturbed in V185N-PSII, or the Mn_4Ca cluster has a modified spin state/structure.

Based on the current knowledge of the Mn_4Ca -cluster and the proposed mechanisms for substrate exchange we discuss these findings and their implications for the overall effects of the V185N-mutation on the S state cycle. The aim is to find the best unifying hypothesis for the substrate exchange and the effects we observe with both TR-MIMS and EPR. In the process, we will consider the current proposals for structural intermediates in the different S states and substrate waters (W_2 , W_3 and O_5) [16,36,37,77–80], and other data from the literature.

4.1. General considerations about substrate exchange and structural intermediates

As a rule of thumb, in order to exchange water bound to a Mn-complex, it should be bound as a terminal and fully protonated ligand on Mn(II) or Mn(III), as Mn(IV) is generally considered to be exchange inert. Additionally, one has to consider that water exchange can occur through two different mechanisms, namely through an associative mechanism, where a new water binds first before the original water ligand leaves, or a dissociative mechanism, where a water is released first before another water binds. Waters bound terminally to Ca^{2+} are considered to always be readily exchangeable with rates that may be considered instantaneous in the time regime of our exchange measurements, as long as no other factors limit their rate of exchange [25,35,37].

As a consequence, for exchanging O_5 (the main candidate for W_s [24,32,37]), it is necessary to consider possible alternative Mn_4Ca cluster structures in addition to the dominant structures resolved for the S_0 – S_3 states using femtosecond serial crystallography [18,29,35–37,81]. In addition, it is important to investigate possible rate limitations for the exchange of W_f that may be imposed by diffusional barriers for bulk water to reach the catalytic site [16,37,82,83].

4.2. On the chemical nature of the valine to asparagine mutation

In order to better rationalize our data, it seems crucial that we first discuss the chemical change we introduced with the V185N mutation. Since valine is a hydrophobic aliphatic residue, it is expected not to interact directly with the surrounding water environment, but may instead pose an obstacle to water movements at or around the cluster. On the basis of calculations it was recently suggested that a change in the orientation of the V185 sidechain away from the crystallographically determined position (see Fig. 1 A & B) may allow to lower the barrier of W_3 insertion from Ca to Mn1 considerably [43]. It is still unclear if this movement of the V185 actually occurs, as it has for example not been observed in recent time-resolved XFEL experiments of PSII [18,81], and if such movements would be dependent or independent of the oxidation state of the Mn_4Ca -cluster.

With the change from a valine to asparagine, a polar headgroup with a high propensity for hydrogen bonding is introduced, potentially involving the amide-N and carbonyl-O as H-bond donors and acceptors, respectively. If an asparagine is inserted instead of the valine and the backbone does not shift, there are a few possibilities for the rotameric state of the asparagine sidechain (see Supplemental Fig. 4). In one of

these rotamers, the amidic headgroup of the sidechain is turned in such a way that either the NH_2 or the O could participate in H-bonding with W_2 , W_3 , O_5 or O_x (Fig. 1C–F). In the S_3 state, it is clear that also the freshly inserted O_x becomes a potential H-bonding candidate (Fig. 1D, F). Alternatively, with a rotation around the $C\alpha$ – $C\beta$ bond, there is the possibility of amidic headgroup of the residue being oriented away from the Mn_4Ca -cluster and towards the chloride channel, where it could interact with the waters or amino acid residues there (see Supplemental Fig. 4). This seems to be the case for the V185T mutant, where the effects of the mutation include altered proton release that were interpreted as effects on the chloride. In addition, the V185T mutation in *T. elongatus* core complex preparations converted the S_2 EPR multiline signal into $g \sim 4$ HS signal [44,75]. This effect is similar to what we observed here with the V185N mutation, which caused a near complete suppression of the S_2 state EPR multiline signal, while the ammonia addition experiment implies that the S_2 state was formed to the same extent in both samples. Due to the ‘binary’ effect on our EPR data we find it, in connection with the changes observed by MIMS in the water exchange rates, most likely that a rotamer of the amino acid residue that is pointing towards the Mn_4Ca -cluster is present in the V185N mutant.

From crystallographic and IR studies, the most likely channel for water access is the $O1$ -channel [18,29,81,84], which is located on the opposite side of the Mn_4Ca -cluster relative to V185. The Cl -channel in the vicinity of V185 has been reported to be primarily important for proton shuffling and release [18,29,81].

4.3. Are the observed effects on the W_s exchange rates a result of shifted conformational equilibria?

Alternative conformations to the ones observed by crystallography have been suggested in all S states [79], and as mentioned above, we previously linked elevated exchange rates of W_s in the S_2 state induced by Ca/Sr substitution and/or high pH to the equilibrium between the low spin and high spin conformation of the Mn_4Ca -cluster. On that basis, we concluded that, of the HS spin conformations proposed (Fig. 2), the one with a ‘prematurely’ bound water ligand (S_2^{AW}) is the most likely one [37]. Although, in the present study, we were unable to detect a high spin EPR signal, the greatly diminished and modified multiline in the V185N mutant and the multiline recovery by addition of ammonia indicate that also in this case the faster W_s exchange may be correlated to a second, faster exchanging conformation of the Mn_4Ca cluster. By analogy, we thus consider an S_2^{AW} type conformation also in this case as the most suitable candidate for explaining the elevated exchange rate of W_s . Since both flash-illumination at room temperature and 200 K illumination of the S_1 state V185N-PSII samples resulted in very small EPR multiline signals, we suggest that in the mutant also the S_1 state attains a modified conformation. However, since the S_1 split signal appears unaltered, the total spin appears to be identical to that in the S_1 state of WT-PSII. The S_1 state exhibits the largest relative difference in exchange rate of W_s between mutant and WT, and thus the presence of a second, faster exchanging structure in the S_1 state would provide a convenient explanation for this finding. Additional S_1 state conformation have already been suggested previously [79,85–87].

Bearing all of this in mind, we move the discussion into the S_3 state. Here, the S_3^{AW} conformation is the most stable structure and there is a broad consensus that all Mn ions are in oxidation state IV [16,88–93]. Therefore, this is also the most difficult S state to rationalize manganese centered water exchange as the manganese coordination is saturated and direct exchange of a water seems excluded. Two suggestions have been made that could potentially alleviate this problem. Firstly, back donation of an electron from Y_Z to the Mn_4Ca cluster may lead to the reduction of the S_3^{AW} state (see Fig. 2) to the $S_2^{AW}Y_Z$ state, which is structurally similar to S_3^{AW} but harbors a Mn(III). In this state, W_f and W_s would exchange exactly as they would in the S_2^{AW} state, regardless if $W_f = O_x$ (previous W_3) or $W_f = W_2$ [35]. In the alternative proposal

for water exchange in S_3 , the S_3^{AW} conformation would convert to the S_3^{BW} conformation (see Fig. 2) [37]. From here, the S_3^B -conformation with a five-coordinated Mn4(IV) may be reached, which would necessitate the release of one water. Reformation of the fully hydrated cluster (S_3^{BW} and subsequently S_3^{AW}) would involve the binding of a new water molecule, and thus result in the exchange of the original water ligand [37]. As shown in Fig. 2 (bottom) this may lead to $W_s = O5$ exchange. We note that this S_3^B water exchange mechanism also promotes the exchange of W_f , but only if W_f were $W2$ (see below). The possibility of the Mn_4Ca cluster to attain the S_3^B conformation was recently experimentally supported by Chrysina et al. on the basis of EDNMR spectroscopy measurements of the S_3 state formed under conditions suggested to limit substrate binding [94].

Thus, with both suggested exchange mechanisms for substrate water in the S_3 state, a stabilization of the S_3^{AW} state would be expected to slow the W_s and W_f exchange rates to the same extent (with the caveat regarding W_f mentioned above). We therefore propose that N185 forms an H-bond with Ox, thereby stabilizing the S_3^{AW} conformation. Interestingly, as will be explained below, this H-bond formation to Ox may also explain the faster W_s exchange in the S_2 state and the stabilization of the EPR 'invisible' S_2 state.

As we discussed in [37], enrichment of the S_2^{AW} conformation could lead to the faster exchange of W_s in the S_2^{HS} state, as it resembles an intermediate in the S_2 state exchange mechanism proposed by Siegbahn [35] (see also ref. [36]). In this mechanism, it is necessary to bind a water to Mn1, which deprotonates so that its oxygen replaces O5, while O5 exchanges with bulk water in a terminal ligand position at Mn4. The rate limiting step would be the water binding event leading to a S_2^{AW} -like conformation (for details see [37]).

Hydrogen bonding of N185 to Ox may also explain why the S_2^{AW} conformation, which was suggested previously to give rise to an S_2^{HS} EPR signal, is more stable and thus why the S_2^{LS} EPR multiline signal amplitude is greatly diminished in the V185N mutant. At the same time, the H-bonding would likely alter the magnetic couplings, rationalizing why the S_2^{HS} and the S_2Y_Z states do not show the expected EPR signals. Additionally, we notice that the N185 residue is located on the same helix as H190. If the helix would be shifted slightly due to hydrogen bond interactions of N185, this could be expected to influence the S_3 split EPR signal, which depends on the H-bond between Y_Z and H190 [95].

In the S_2 state, the rates of W_s exchange in the V185N mutant is 2 times faster than in WT-PSII. This is a relatively small effect as compared to the 10-fold acceleration of W_s exchange obtained by stabilizing S_2^{HS} in WT-PSII by high pH observed in our recent study [37]. This can be accounted for by the different type of stabilization of the S_2^{AW} conformation by N185 in mutant-PSII as compared to pH 8.6 in WT-PSII. Additionally, small differences in the structures of the S_2^{HS} conformations likely contribute to the different extent of the effects on the water exchange rates. Following our previous analysis [37], we suggest that starting from the S_2^{AW} state, a conformational change into the S_2^{BW} conformation is necessary so that O5 becomes a terminal ligand on Mn4(III) and thereby exchangeable with bulk water (see Fig. 2).

Thus, the assumption that the D1-V185N mutation stabilizes a S_2^{AW} -like structure in the S_2 state and the S_3^{AW} conformation in the S_3 state leads to a simple and consistent explanation of water exchange assuming O5 is the slowly exchanging substrate water W_s . It is tempting to extend this explanation to the S_1 state where we observed four-fold difference in the W_s exchange rates between WT and V185N-PSII. This would imply the existence of a water-bound form of S_1 , such as for example a S_1^{AW} state. However, too little structural and/or spectroscopic data are at hand presently to support this idea.

In addition to O5, W2 was also presented as option for W_s in instances where a nucleophilic attack mechanism between W3 and W2, or a geminal coupling on Mn4 are proposed for O—O bond formation [19,24,54,96–99]. As we outlined in our recent paper [37], to explain how the exchange rate of W2 would accelerate with the conformational

change from S_2^{LS} to S_2^{HS} it is required that the S_2^{HS} state has a S_2^B (closed cubane) like conformation in the S_2 state (Fig. 2). Then W2 would be bound to the five-coordinate Mn4(III) in the S_2^B state, which would make it easily exchangeable. W2 exchange in the S_1 state would be slower, since then W2 would be bound in the dominant S_1^A form to the six coordinate Mn4(III), and in contrast to S_2 the S_1^B form is high in energy. Thus, to explain the effects on water exchange and EPR signals observed in this study, the V185N mutation would need to stabilize the S_1^B and S_2^B conformations over the corresponding A-type conformations. We find this less plausible as compared to the stabilization of the S_2^{AW} conformation, as the positions of O5 in S_2^A and S_2^B is rather similar.

4.4. Exchange of W_f

W2 and W3 have both been suggested as candidates for the fast exchanging substrate W_f in the S_2 state. In case of W3, a binding to either Mn1 or Mn4 during the $S_2 \rightarrow S_3$ transition was proposed [16,18,24,55,77,81,100–103].

Our experiments show that, in the S_3 state, the exchange of W_f is, just as for W_s , two-fold slower in the V185N-PSII than in WT-PSII. Independent of the substrate water exchange mechanism, this similar slowing is strong evidence that both substrate waters are bound to Mn (IV) ions in the S_3 state. In case that substrate exchange is facilitated by electron donation by Y_Z to the Mn_4Ca cluster, our results do not allow a further discrimination between the two options for W_f . However, if water exchange in S_3 involves the S_3^B state, the similar slowing caused by the mutation favors that W_f is bound to Mn4 in the S_3 state, as its exchange will then depend on the same equilibrium that regulates W_s exchange. This would favor W2 as W_f , or that W3 binds to Mn4 during the $S_2 \rightarrow S_3$ transition.

In the S_2 state, the exchange rate of W_f is essentially identical for both WT-PSII and V185N-PSII. As explained in the following, this may be best understood if water diffusion through the channels to the catalytic site is limiting the exchange rate of W_f in the S_2 state.

Firstly, if W_f were W2, W_f exchange would be expected to be affected by the shifted structural equilibrium in S_2 induced by the mutation. For example, W2 is bound to Mn4(IV) in the S_2^A state that is dominant in WT-PSII, while it is bound to Mn4(III) in the S_2^{AW} state that we propose is stabilized in the mutant. The same would be true if the V185N mutation would stabilize the S_2^B state. Although the oxidation state assignment for the S_2^{HS} state stabilized by the mutation is uncertain, since we did not observe the HS EPR signal, the absence of observed differences in W_f exchange in the S_2 state favors that either W_f is W3 (see below), or that W2 exchanges so fast in both the S_2^A and S_2^{AW} states that its exchange rate is limited by the diffusion of labelled water through the water channels leading from the surface of PSII to the Mn_4Ca cluster [24].

Secondly, if the Ca-bound W3 water molecule was W_f in the S_2 state, then the independence of its exchange rate in the S_2 state from the conformation of the Mn_4Ca cluster would be straight forward to understand. However, as Ca-bound water should exchange instantaneously with respect to the time-resolution in our experiments, also this scenario requires that the diffusion of water through the access channels would limit the rate of W_f exchange. Thus, even some expected differences in H-bonding of W3 caused by the mutation would not result in any difference on the exchange rate.

We note that while it was shown previously that (i) the rate of reduction of the Mn_4Ca cluster by derivatives of hydroxylamine and hydrazine depends on their molecular dimensions [104], and (ii) that there are barriers for water diffusion in all channels [83,105], evidence that water access to the catalytic site is limiting the exchange of W_f is still lacking. In addition, the lack of resolving W_f exchange in the S_1 state would need to be explained by its isotopic scrambling with bulk water during the dark-times between subsequent flashes required for O_2 formation. Calculations shown in the supporting information indicate

that this may be the case.

5. Conclusion

The altered substrate water exchange kinetics caused by the replacement of D1 valine 185 by asparagine can be consistently explained by assuming that asparagine forms a hydrogen bond with Ox and thereby stabilizes the S_3^{AW} and S_2^{AW} , and possibly even S_1^{AW} , conformations. Since DFT calculations and our recent substrate water exchange data suggest that these states are key intermediates for O₅ exchange [35,37], our data provide strong support for the proposal that O₅ is W_s. The present data are most easily explained by the assumption that W_f exchange in the S_2 state is access limited, thus no further conclusion on its binding site in the S_2 state can be derived. In contrast, the data strongly support that W_f is bound to Mn in the S_3 state. These preferred assignments of W_f and W_s support O–O bond formation by radical coupling between Ox and O₅, in either the open or closed cube conformation [24,27].

Declaration of competing interest

The authors declare that they have no known competing financial interests or personal relationships that could have appeared to influence the work reported in this paper.

Acknowledgements

The authors appreciate the help of Mohammed Ibrahim for technical assistance in depiction of the crystallographic models in the S_3 state and Mun Hon Cheah for valuable discussions and technical advice concerning the TR-MIMS experiments.

Funding

Financial support was provided by Vetenskabsrådet (grant number: 2016-05183) and the National Science Foundation NSF (MCB-1716408).

Appendix A. Supplementary data

Supplementary data to this article can be found online at <https://doi.org/10.1016/j.bbabo.2020.148319>.

References

- [1] N. Nelson, W. Junge, Structure and energy transfer in photosystems of oxygenic photosynthesis, *Annu. Rev. Biochem.* 84 (2015) 659–683.
- [2] J.-R. Shen, The structure of photosystem II and the mechanism of water oxidation in photosynthesis, *Annu. Rev. Plant Biol.* 66 (2015) 23–48.
- [3] J. Barber, Photosystem II: the water splitting enzyme of photosynthesis and the origin of oxygen in our atmosphere, *Q. Rev. Biophys.* 49 (2016) 1–21.
- [4] W. Junge, Oxygenic photosynthesis: history, status and perspective, *Q. Rev. Biophys.* 52 (2019) 1–17.
- [5] W. Lubitz, M. Chrysina, N. Cox, Water oxidation in photosystem II, *Photosynth. Res.* 142 (2019) 105–125.
- [6] G.T. Babcock, B.A. Barry, R.J. Debus, C.W. Hoganson, M. Atamian, L. McIntosh, I. Sithole, C.F. Yocum, Water oxidation in photosystem II: from radical chemistry to multielectron chemistry, *Biochemistry* 28 (1989) 9557–9565.
- [7] T. Cardona, A. Sedoud, N. Cox, A.W. Rutherford, Charge separation in photosystem II: a comparative and evolutionary overview, *Biochem. Biophys. Acta - Bioenerg.* 1817 (2012) 26–43.
- [8] G. Renger, Chapter 16 Functional pattern of photosystem II, *Primary Processes of Photosynthesis, Part 2: Principles and Apparatus*, The Royal Society of Chemistry, 2008, pp. 237–290.
- [9] P. Joliot, G. Barbieri, R. Chabaud, Un nouveau modele des centres photochimiques du systeme II, *Photochem. Photobiol.* 10 (1969) 309–329.
- [10] B. Kok, B. Forbush, M. McGloin, Cooperation of charges in photosynthetic O₂ evolution - I. A linear four step mechanism, *Photochem. Photobiol.* 11 (1970) 457–475.
- [11] B.A. Diner, Dependence of the deactivation reactions of photosystem II on the redox state of plastoquinone pool A varied under anaerobic conditions. *Equilibria on the acceptor side of photosystem II*, *Biochem. Biophys. Acta - Bioenerg.* 460 (1977) 247–258.
- [12] H.H. Robinson, A.R. Crofts, Kinetics of the oxidation-reduction reactions of the photosystem II quinone acceptor complex, and the pathway for deactivation, *FEBS Lett.* 153 (1983) 221–226.
- [13] J. Messinger, G. Renger, Chapter 17 Photosynthetic water splitting, in: G. Renger (Ed.), *Primary Processes of Photosynthesis, Part 2: Principles and Apparatus*, The Royal Society of Chemistry, 2008, pp. 291–349.
- [14] T. Noguchi, FTIR detection of water reactions in the oxygen-evolving centre of photosystem II, *Philos. Trans. Soc., B* 363 (2008) 1189–1195.
- [15] L. Rapatskiy, N. Cox, A. Savitsky, W.M. Ames, J. Sander, M.M. Nowaczyk, M. Rögner, A. Boussac, F. Neese, J. Messinger, W. Lubitz, Detection of the water-binding sites of the oxygen-evolving complex of photosystem II using W-band ¹⁷O electron-electron double resonance-detected NMR spectroscopy, *J. Am. Chem. Soc.* 134 (2012) 16619–16634.
- [16] N. Cox, J. Messinger, Reflections on substrate water and dioxygen formation, *Biochem. Biophys. Acta - Bioenerg.* 1827 (2013) 1020–1030.
- [17] R.J. Debus, FTIR studies of metal ligands, networks of hydrogen bonds, and water molecules near the active site Mn₄CaO₅ cluster in photosystem II, *Biochem. Biophys. Acta - Bioenerg.* 1847 (2014) 19–34.
- [18] J. Kern, R. Chatterjee, I.D. Young, F.D. Fuller, L. Lassalle, M. Ibrahim, S. Gul, T. Fransson, A.S. Brewster, R. Alonso-Mori, R. Hussein, M. Zhang, L. Douthit, C. de Lichtenberg, M.H. Cheah, D. Shevela, J. Wersig, I. Seuffert, D. Sokaras, E. Pastor, C. Weninger, T. Kroll, R.G. Sierra, P. Aller, A. Butryn, A.M. Orville, M. Liang, A. Batyuk, J.E. Koglin, S. Carbajo, S. Boutet, N.W. Moriarty, J.M. Holton, H. Dobbek, P.D. Adams, U. Bergmann, N.K. Sauter, A. Zouni, J. Messinger, J. Yano, V.K. Yachandra, Structures of the intermediates of Kok's photosynthetic water oxidation clock, *Nature* 563 (2018) 421–425.
- [19] J. Messinger, M. Badger, T. Wydrzynski, Detection of one slowly exchanging substrate water molecule in the S_3 state of photosystem II, *Proc. Natl. Acad. Sci. U.S.A.* 92 (1995) 3209–3213.
- [20] L. Konermann, J. Messinger, W. Hillier, Mass spectrometry-based methods for studying kinetics and dynamics in biological systems, in: T.J. Artsma and J. Matysik (Eds.), *Biophysical Techniques in Photosynthesis*, Springer, Dordrecht, 2008, pp. 167–190.
- [21] K. Beckmann, J. Messinger, M.R. Badger, T. Wydrzynski, W. Hillier, On-line mass spectrometry: membrane inlet sampling, *Photosynth. Res.* 102 (2009) 511–522.
- [22] D. Shevela, J. Messinger, Studying the oxidation of water to molecular oxygen in photosynthetic and artificial systems by time-resolved membrane-inlet mass spectrometry, *Front. Plant Sci.* 4 (2013) 1–9.
- [23] W. Hillier, T. Wydrzynski, Oxygen ligand exchange at metal sites - implications for the O₂ evolving mechanism of photosystem II, *Biochem. Biophys. Acta - Bioenerg.* 1503 (2001) 197–209.
- [24] J. Messinger, Evaluation of different mechanistic proposals for water oxidation in photosynthesis on the basis of Mn₄O_xCa structures for the catalytic site and spectroscopic data, *Phys. Chem. Chem. Phys.* 6 (2004) 4764–4771.
- [25] W. Hillier, T. Wydrzynski, ¹⁸O-water exchange in photosystem II: substrate binding and intermediates of the water splitting cycle, *Coord. Chem. Rev.* 252 (2008) 306–317.
- [26] T. Noguchi, M. Sugiura, Flash-induced FTIR difference spectra of the water oxidizing complex in moderately hydrated photosystem II core films: effect of hydration extent on S-state transitions, *Biochemistry* 41 (2002) 2322–2330.
- [27] P.E.M. Siegbahn, Structures and energetics for O₂ formation in photosystem II, *Acc. Chem. Res.* 42 (2009) 1871–1880.
- [28] H. Yata, T. Noguchi, Mechanism of methanol inhibition of photosynthetic water oxidation as studied by Fourier transform infrared difference and time-resolved infrared spectroscopies, *Biochemistry* 57 (2018) 4803–4815.
- [29] M. Suga, F. Akita, K. Yamashita, Y. Nakajima, G. Ueno, H. Li, T. Yamane, K. Hirata, Y. Umena, S. Yonekura, L.-J. Yu, H. Murakami, T. Nomura, T. Kimura, M. Kubo, S. Baba, T. Kumasaka, K. Tono, M. Yabashi, H. Isobe, K. Yamaguchi, M. Yamamoto, H. Ago, J.-R. Shen, An oxy/oxo mechanism for oxygen-oxygen coupling in PSII revealed by an X-ray free-electron laser, *Science* 366 (2019) 334.
- [30] Y. Umena, K. Kawakami, J.-R. Shen, N. Kamiya, Crystal structure of oxygen-evolving photosystem II at a resolution of 1.9 Å, *Nature* 473 (2011) 55–60.
- [31] M. Suga, F. Akita, M. Sugahara, M. Kubo, Y. Nakajima, T. Nakane, K. Yamashita, Y. Umena, M. Nakabayashi, T. Yamane, T. Nakano, M. Suzuki, T. Masuda, S. Inoue, T. Kimura, T. Nomura, S. Yonekura, L.-J. Yu, T. Sakamoto, T. Motomura, J.-H. Chen, Y. Kato, T. Noguchi, K. Tono, Y. Joti, T. Kameshima, T. Hatsui, E. Nango, R. Tanaka, H. Naitow, Y. Matsuura, A. Yamashita, M. Yamamoto, O. Nureki, M. Yabashi, T. Ishikawa, S. Iwata, J.-R. Shen, Light-induced structural changes and the site of O=O bond formation in PSII caught by XFEL, *Nature* 543 (2017) 131–135.
- [32] P.E.M. Siegbahn, O–O bond formation in the S_4 state of the oxygen-evolving complex in photosystem II, *Chem.: Eur. J.* 12 (2006) 9217–9227.
- [33] M. Perez Navarro, W.M. Ames, H. Nilsson, T. Lohmiller, D.A. Pantazis, L. Rapatskiy, M.M. Nowaczyk, F. Neese, A. Boussac, J. Messinger, W. Lubitz, N. Cox, Ammonia binding to the oxygen-evolving complex of photosystem II identifies the solvent-exchangeable oxygen bridge (μ-oxo) of the manganese tetramer, *Proc. Natl. Acad. Sci. U.S.A.* 110 (2013) 15561–15566.
- [34] T. Lohmiller, V. Krewald, A. Sedoud, A.W. Rutherford, F. Neese, W. Lubitz, D.A. Pantazis, N. Cox, The first state in the catalytic cycle of the water-oxidizing enzyme: identification of a water-derived μ-hydroxo bridge, *J. Am. Chem. Soc.* 139 (2017) 14412–14424.
- [35] P.E.M. Siegbahn, Substrate water exchange for the oxygen evolving complex in PSII in the S_1 , S_2 , and S_3 states, *J. Am. Chem. Soc.* 135 (2013) 9442–9449.
- [36] Y. Guo, H. Li, L.-L. He, D.-X. Zhao, L.-D. Gong, Z.-Z. Yang, Theoretical reflections

- on the structural polymorphism of the oxygen-evolving complex in the S_2 state and the correlations to substrate water exchange and water oxidation mechanism in photosynthesis, *Biochem. Biophys. Acta - Bioenerg.* 1858 (2017) 833–846.
- [37] C. de Lichtenberg, J. Messinger, Substrate water exchange in the S_2 state of photosystem II is dependent on the conformation of the Mn_4Ca cluster, *Phys. Chem. Chem. Phys.* 22 (2020) 12894–12908.
- [38] R.J. Debus, The catalytic manganese cluster: protein ligation, in: T.J. Wydrzynski, K. Satoh, J.A. Freeman (Eds.), *Photosystem II: The Light-driven Water:Plastoquinone Oxidoreductase*, Springer, Dordrecht, 2005, pp. 261–284.
- [39] R.J. Debus, FTIR studies of metal ligands, networks of hydrogen bonds, and water molecules near the active site Mn_4CaO_5 cluster in Photosystem II, *Biochem. Biophys. Acta - Bioenerg.* 1847 (2015) 19–34.
- [40] P.L. Dilbeck, H. Bao, C.L. Neveu, R.L. Burnap, Perturbing the water cavity surrounding the manganese cluster by mutating the residue D1-valine 185 has a strong effect on the water oxidation mechanism of photosystem II, *Biochemistry* 52 (2013) 6824–6833.
- [41] H. Bao, R.L. Burnap, Structural rearrangements preceding dioxygen formation by the water oxidation complex of photosystem II, *Proc. Natl. Acad. Sci. U.S.A.* 112 (2015) E6139–E6147.
- [42] C.J. Kim, H. Bao, R.L. Burnap, R.J. Debus, Impact of D1-V185 on the water molecules that facilitate O_2 formation by the catalytic Mn_4CaO_5 cluster in photosystem II, *Biochemistry* 57 (2018) 4299–4311.
- [43] P.E.M. Siegbahn, The S_2 to S_3 transition for water oxidation in PSII (photosystem II), revisited, *Phys. Chem. Chem. Phys.* 20 (2018) 22926–22931.
- [44] M. Sugiura, T. Tibiletti, I. Takachi, Y. Hara, S. Kanawaku, J. Sellés, A. Boussac, Probing the role of valine 185 of the D1 protein in the photosystem II oxygen evolution, *Biochem. Biophys. Acta - Bioenerg.* 1859 (2018) 1259–1273.
- [45] A. Boussac, Temperature dependence of the high-spin S_2 to S_3 transition in photosystem II: mechanistic consequences, *Biochem. Biophys. Acta - Bioenerg.* 1860 (2019) 508–518.
- [46] R.D. Britt, K.A. Campbell, J.M. Peloquin, M.L. Gilchrist, C.P. Aznar, M.M. Dicus, J. Robblee, J. Messinger, Recent pulsed EPR studies of the photosystem II oxygen-evolving complex: implications as to water oxidation mechanisms, *Biochem. Biophys. Acta - Bioenerg.* 1655 (2004) 158–171.
- [47] V. Petrouleas, D. Koulougliotis, N. Ioannidis, Trapping of metalloradical intermediates of the S-states at liquid helium temperatures. Overview of the phenomenology and mechanistic implications, *Biochemistry* 44 (2005) 6723–6728.
- [48] A. Haddy, EPR spectroscopy of the manganese cluster of photosystem II, *Photosynth. Res.* 92 (2007) 357–368.
- [49] G.C. Dismukes, Y. Siderer, Intermediates of a polynuclear manganese center involved in photosynthetic oxidation of water, *Proc. Natl. Acad. Sci. U.S.A.* 78 (1981) 274–278.
- [50] Ö. Hansson, L.-E. Andréasson, EPR-detectable magnetically interacting manganese ions in the photosynthetic oxygen-evolving system after continuous illumination, *Biochem. Biophys. Acta - Bioenerg.* 679 (1982) 261–268.
- [51] J.L. Casey, K. Sauer, EPR detection of a cryogenically photogenerated intermediate in photosynthetic oxygen evolution, *Biochem. Biophys. Acta - Bioenerg.* 767 (1984) 21–28.
- [52] J.L. Zimmermann, A.W. Rutherford, Electron paramagnetic resonance properties of the S_2 state of the oxygen-evolving complex of photosystem II, *Biochemistry* 25 (1986) 4609–4615.
- [53] D.A. Pantazis, W. Ames, N. Cox, W. Lubitz, F. Neese, Two interconvertible structures that explain the spectroscopic properties of the oxygen-evolving complex of photosystem II in the S_2 state, *Angew. Chem. Int. Ed.* 51 (2012) 9935–9940.
- [54] H. Isobe, M. Shoji, S. Yamanaka, Y. Umena, K. Kawakami, N. Kamiya, J.-R. Shen, K. Yamaguchi, Theoretical illumination of water-inserted structures of the $CaMn_4O_5$ cluster in the S_2 and S_3 states of oxygen-evolving complex of photosystem II: full geometry optimizations by B3LYP hybrid density functional, *Dalton Trans.* 41 (2012) 13727–13740.
- [55] D. Bovi, D. Narzi, L. Guidoni, The S_2 state of the oxygen-evolving complex of photosystem II explored by QM/MM dynamics: spin surfaces and metastable states suggest a reaction path towards the S_3 state, *Angew. Chem. Int. Ed.* 52 (2013) 11744–11749.
- [56] K. Miyagawa, H. Isobe, T. Kawakami, M. Shoji, S. Yamanaka, M. Okumura, T. Nakajima, K. Yamaguchi, Domain-based local pair natural orbital CCSD(T) calculations of fourteen different S_2 intermediates for water oxidation in the Kok cycle of OEC of PSII. Re-visit to one LS-two HS model for the S_2 state, *Chem. Phys. Lett.* 734 (2019) 136731.
- [57] Y. Pushkar, A.K. Ravari, S.C. Jensen, M. Palenik, Early binding of substrate oxygen is responsible for a spectroscopically distinct S_2 state in photosystem II, *J. Phys. Chem. Lett.* 10 (2019) 5284–5291.
- [58] T.A. Corry, P.J. O'Malley, Proton isomers rationalize the high- and low-spin forms of the S_2 state intermediate in the water-oxidizing reaction of photosystem II, *J. Phys. Chem. Lett.* 10 (2019) 5226–5230.
- [60] R. Chatterjee, G. Han, J. Kern, S. Gul, F.D. Fuller, A. Garachtchenko, I.D. Young, T.-C. Weng, D. Nordlund, R. Alonso-Mori, U. Bergmann, D. Sokaras, M. Hatakeyama, V.K. Yachandra, J. Yano, Structural changes correlated with magnetic spin state isomorphism in the S_2 state of the Mn_4CaO_5 cluster in the oxygen-evolving complex of photosystem II, *Chem. Sci.* 7 (2016) 5236–5248.
- [61] R. Chatterjee, L. Lassalle, S. Gul, F.D. Fuller, I.D. Young, M. Ibrahim, C. de Lichtenberg, M.H. Cheah, A. Zouni, J. Messinger, V.K. Yachandra, J. Kern, J. Yano, Structural isomers of the S_2 state in photosystem II: do they exist at room temperature and are they important for function? *Physiol. Plant.* 166 (2019) 60–72.
- [62] M.A. Strickler, L.M. Walker, W. Hillier, R.J. Debus, Evidence from biosynthetically incorporated strontium and FTIR difference spectroscopy that the C-terminus of the D1 polypeptide of photosystem II does not ligate calcium, *Biochemistry* 44 (2005) 8571–8577.
- [63] R.J. Porra, W.A. Thompson, P.E. Kriedemann, Determination of accurate extinction coefficients and simultaneous equations for assaying chlorophylls a and b extracted with four different solvents: verification of the concentration of chlorophyll standards by atomic absorption spectroscopy, *Biochem. Biophys. Acta - Bioenerg.* 975 (1989) 384–394.
- [64] X.-S. Tang, B.A. Diner, Biochemical and spectroscopic characterization of a new oxygen-evolving photosystem II core complex from the cyanobacterium *Synechocystis PCC 6803*, *Biochemistry* 33 (1994) 4594–4603.
- [65] W. Hillier, J. Messinger, T. Wydrzynski, Kinetic determination of the fast exchanging substrate water molecule in the S_3 state of photosystem II, *Biochemistry* 37 (1998) 16908–16914.
- [66] D. Shevela, W.P. Schröder, J. Messinger, Liquid-Phase Measurements of Photosynthetic Oxygen Evolution, in: S. Govshoff (Ed.), *Photosynthesis: Methods and Protocols, Methods in Molecular Biology*, 1770 Springer, New York, NY, 2018, pp. 197–211.
- [67] H. Nilsson, T. Krupnik, J. Kargul, J. Messinger, Substrate water exchange in photosystem II core complexes of the extremophilic red alga *Cyanidioschyzon merolae*, *Biochem. Biophys. Acta - Bioenerg.* 1837 (2014) 1257–1262.
- [68] H. Nilsson, Substrate Water Binding to the Oxygen-evolving Complex in Photosystem II, PhD thesis, Umeå Universitet, 2014.
- [69] W. Hillier, T. Wydrzynski, The affinities for the two substrate water binding sites in the O_2 evolving complex of photosystem II vary independently during S-state turnover, *Biochemistry* 39 (2000) 4399–4405.
- [70] W. Hillier, G. Hendry, R.L. Burnap, T. Wydrzynski, Substrate water exchange in photosystem II depends on the peripheral proteins, *J. Biol. Chem.* 276 (2001) 46917–46924.
- [71] W. Hillier, I. McConnell, S. Singh, R. Debus, A. Boussac, T. Wydrzynski, Substrate water oxygen exchange in photosystem II: insights from mutants and Ca vs. Sr substitution, in: J.F. Allen, E. Gantt, J.H. Golbeck, B. Osmond (Eds.), *Photosynthesis. Energy from the Sun: 14th International Congress on Photosynthesis*, Springer, 2008, pp. 427–430.
- [72] K.G.V. Havelius, J.-H. Su, Y. Feyziyev, F. Mamedov, S. Styring, Spectral resolution of the split EPR signals induced by illumination at 5 K from the S_1 , S_3 , and S_0 states in photosystem II, *Biochemistry* 45 (2006) 9279–9290.
- [73] A. Boussac, M. Sugiura, Y. Inoue, A.W. Rutherford, EPR study of the oxygen evolving complex in his-tagged photosystem II from the cyanobacterium *Synechococcus elongatus*, *Biochemistry* 39 (2000) 13788–13799.
- [74] K.V. Lakshmi, M.J. Reifler, D.A. Chisholm, J.Y. Wang, B.A. Diner, G.W. Brudvig, Correlation of the cytochrome c_2 content of cyanobacterial photosystem II with the EPR properties of the oxygen-evolving complex, *Photosynth. Res.* 72 (2002) 175–189.
- [75] A. Boussac, I. Ugur, A. Marion, M. Sugiura, V.R.I. Kaila, A.W. Rutherford, The low spin - high spin equilibrium in the S_2 -state of the water oxidizing enzyme, *Biochem. Biophys. Acta - Bioenerg.* 1859 (2018) 342–356.
- [76] N. Ioannidis, V. Petrouleas, Electron paramagnetic resonance signals from the S_3 state of the oxygen-evolving complex. A broadened radical signal induced by low-temperature near-infrared light illumination, *Biochemistry* 39 (2000) 5246–5254.
- [77] D.J. Vinyard, G.W. Brudvig, Progress toward a molecular mechanism of water oxidation in photosystem II, *Annu. Rev. Phys. Chem.* 68 (2017) 101–116.
- [78] Y. Guo, H. Li, L.-L. He, D.-X. Zhao, L.-D. Gong, Z.-Z. Yang, The open-cubane oxo-oxyl coupling mechanism dominates photosynthetic oxygen evolution: a comprehensive DFT investigation on O–O bond formation in the S_4 state, *Phys. Chem. Chem. Phys.* 19 (2017) 13909–13923.
- [79] D.A. Pantazis, Missing pieces in the puzzle of biological water oxidation, *ACS Catal.* 8 (2018) 9477–9507.
- [80] N. Cox, D.A. Pantazis, W. Lubitz, Current understanding of the mechanism of water oxidation in photosystem II and its relation to XFEL data, *Annu. Rev. Biochem.* 89 (2020) 795–820.
- [81] M. Ibrahim, T. Fransson, R. Chatterjee, M.H. Cheah, R. Hussein, L. Lassalle, K.D. Sutherlin, I.D. Young, F.D. Fuller, S. Gul, I.-S. Kim, P.S. Simon, C. de Lichtenberg, P. Chernev, I. Bogacz, C.C. Pham, A.M. Orville, N. Saichek, T. Northen, A. Batyuk, S. Carbajo, R. Alonso-Mori, K. Tono, S. Owada, A. Bhowmick, R. Bolotovskiy, D. Mendez, N.W. Moriarty, J.M. Holton, H. Dobbek, A.S. Brewster, P.D. Adams, N.K. Sauter, U. Bergmann, A. Zouni, J. Messinger, J. Kern, V.K. Yachandra, J. Yano, Untangling the sequence of events during the $S_2 \rightarrow S_3$ transition in photosystem II and implications for the water oxidation mechanism, *Proc. Natl. Acad. Sci. U.S.A.* 117 (23) (2020) 12624–12635.
- [82] F.M. Ho, S. Styring, Access channels and methanol binding site to the $CaMn_4$ cluster in photosystem II based on solvent accessibility simulations, with implications for substrate water access, *Biochem. Biophys. Acta - Bioenerg.* 1777 (2008) 140–153.
- [83] S. Vassiliev, T. Zaraiskaya, D. Bruce, Exploring the energetics of water permeation in photosystem II by multiple steered molecular dynamics simulations, *Biochem. Biophys. Acta - Bioenerg.* 1817 (2012) 1671–1678.
- [84] Y. Shimada, T. Kitajima-Ihara, R. Nagao, T. Noguchi, Role of the O4 channel in photosynthetic water oxidation as revealed by fourier transform infrared difference and time-resolved infrared analysis of the D1-S169A mutant, *J. Phys. Chem. B* 124 (2020) 1470–1480.
- [85] A. Boussac, F. Rappaport, P. Carrier, J.M. Verbavatz, R. Gobin, D. Kirilovsky, A.W. Rutherford, M. Sugiura, Biosynthetic Ca^{2+}/Sr^{2+} exchange in the photosystem II oxygen-evolving enzyme of *Thermosynechococcus elongatus*, *J. Biol. Chem.* 279 (2004) 22809–22819.
- [86] G. Sioros, D. Koulougliotis, G. Karapanagos, V. Petrouleas, The S_1Y_2 metalloradical EPR signal of photosystem II contains two distinct components that advance respectively to the multiline and $g = 4.1$ conformations of S_2 , *Biochemistry* 46

- (2007) 210–217.
- [87] M. Kusunoki, S_1 -state Mn_4Ca complex of photosystem II exists in equilibrium between the two most-stable isomeric substates: XRD and EXAFS evidence, *J. Photochem. Photobiol. B* 104 (2011) 100–110.
- [88] H. Dau, I. Zaharieva, M. Haumann, F. Armstrong, L. Que, Recent developments in research on water oxidation by photosystem II, *Curr. Opin. Chem. Biol.* 16 (2012) 3–10.
- [89] N. Cox, M. Retegan, F. Neese, D.A. Pantazis, A. Boussac, W. Lubitz, Electronic structure of the oxygen-evolving complex in photosystem II prior to O-O bond formation, *Science* 345 (2014) 804–808.
- [90] V. Krewald, M. Retegan, N. Cox, J. Messinger, W. Lubitz, S. DeBeer, F. Neese, D.A. Pantazis, Metal oxidation states in biological water splitting, *Chem. Sci.* 6 (2015) 1676–1695.
- [91] I. Zaharieva, P. Chernev, G. Berggren, M. Anderlund, S. Styring, H. Dau, M. Haumann, Room-temperature energy-sampling K β X-ray emission spectroscopy of the Mn_4Ca complex of photosynthesis reveals three manganese-centered oxidation steps and suggests a coordination change prior to O_2 formation, *Biochemistry* 55 (2016) 4197–4211.
- [92] D.A. Pantazis, The S_3 state of the oxygen-evolving complex: overview of spectroscopy and XFEL crystallography with a critical evaluation of early-onset models for O-O bond formation, *Inorganics* 7 (2019) 55.
- [93] M.H. Cheah, M. Zhang, D. Shevela, F. Mamedov, A. Zouni, J. Messinger, Assessment of the manganese cluster's oxidation state via photoactivation of photosystem II microcrystals, *Proc. Natl. Acad. Sci. U.S.A.* 117 (2020) 141–145.
- [94] M. Chrysina, E. Heyno, Y. Kutin, M. Reus, H. Nilsson, M.M. Nowaczyk, S. DeBeer, F. Neese, J. Messinger, W. Lubitz, N. Cox, Five-coordinate Mn^{IV} intermediate in the activation of nature's water splitting cofactor, *Proc. Natl. Acad. Sci. U.S.A.* 116 (2019) 16841–16846.
- [95] S. Styring, J. Sjöholm, F. Mamedov, Two tyrosines that changed the world: interfacing the oxidizing power of photochemistry to water splitting in photosystem II, *Biochem. Biophys. Acta - Bioenerg.* 1817 (2012) 76–87.
- [96] J.P. McEvoy, G.W. Brudvig, Water-splitting chemistry of photosystem II, *Chem. Rev.* 106 (2006) 4455–4483.
- [97] M. Kusunoki, Mono-manganese mechanism of the photosystem II water splitting reaction by a unique Mn_4Ca cluster, *Biochem. Biophys. Acta - Bioenerg.* 1767 (2007) 484–492.
- [98] E.M. Sproviero, J.A. Gascón, J.P. McEvoy, G.W. Brudvig, V.S. Batista, Quantum mechanics/molecular mechanics study of the catalytic cycle of water splitting in photosystem II, *J. Am. Chem. Soc.* 130 (2008) 3428–3442.
- [99] B. Zhang, L. Sun, Why nature chose the Mn_4CaO_5 cluster as water-splitting catalyst in photosystem II: a new hypothesis for the mechanism of O-O bond formation, *Dalton Trans.* 47 (2018) 14381–14387.
- [100] I. Ugur, A.W. Rutherford, V.R.I. Kaila, Redox-coupled substrate water re-organization in the active site of Photosystem II - the role of calcium in substrate water delivery, *Biochem. Biophys. Acta - Bioenerg.* 1857 (2016) 740–748.
- [101] C.J. Kim, R.J. Debus, Evidence from FTIR difference spectroscopy that a substrate H_2O molecule for O_2 formation in photosystem II is provided by the Ca ion of the catalytic Mn_4CaO_5 cluster, *Biochemistry* 56 (2017) 2558–2570.
- [102] C.J. Kim, R.J. Debus, One of the substrate waters for O_2 formation in Photosystem II is provided by the water-splitting Mn_4CaO_5 cluster's Ca^{2+} ion, *Biochemistry* 58 (2019) 3185–3192.
- [103] H. Sakamoto, T. Shimizu, R. Nagao, T. Noguchi, Monitoring the reaction process during the $S_2 \rightarrow S_3$ transition in photosynthetic water oxidation using time-resolved infrared spectroscopy, *J. Am. Chem. Soc.* 139 (2017) 2022–2029.
- [104] R. Radmer, O. Ollinger, Topography of the O_2 -evolving site determined with water analogs, *FEBS Lett.* 152 (1983) 39–43.
- [105] F.M. Ho, Uncovering channels in photosystem II by computer modelling: current progress, future prospects, and lessons from analogous systems, *Photosynth. Res.* 98 (2008) 503–522.